Available online at www.sciencedirect.com

ScienceDirect

Progress in Natural Science: Materials International 24 (2014) 128–133

Progress in Natural Science Materials International

www.elsevier.com/locate/pnsmi
www.sciencedirect.com

Original Research

Improving the mid-infrared energy absorption efficiency by using a dual-band metamaterial absorber

Nan Zhang, Peiheng Zhou*, Shifeng Zou, Xiaolong Weng, Jianliang Xie, Longjiang Deng

State Key Laboratory of Electronic Thin Films and Integrated Devices, University of Electronic Science and Technology of China, Chengdu 610054, China

Received 26 September 2013; accepted 2 December 2013
Available online 29 April 2014

Abstract

In this paper, a dual-band mid-infrared metamaterial absorber was proposed to improve the energy absorption efficiency. Up to 99% absorption was obtained at 9.03 and 11.83 μm in the simulation, and each absorption band can be tuned by the dielectric spacing layer, i.e., the dielectric constant and its thickness. The dual-band absorption mechanism was analyzed, and the quite well absorption performance at large incident angles was also presented. The results of this study can be applied in the field of thermal absorbing and solar energy harvesting.

Keywords: Metamaterial absorber; Thermal absorption; Solar energy harvesting; Mid-infrared

1. Introduction

Metamaterial absorbers (MAs) have artificial periodic electromagnetic structures, which could achieve a high absorption over a large portion of the electromagnetic spectrum, from radio [1], microwave [2], millimeter wave [3], terahertz [4], infrared [5], to optical regimes [6]. Due to their high absorption efficiency, less thickness, and tunable resonant response, MAs have been taken as ideal candidates for applications including sensors [7], solar cells [8,9], thermal emitters [10,11], and imaging devices [12]. However, most of these MAs are single-band structures with a narrow bandwidth, since the effective absorption is based on the strong electromagnetic resonance to the incident light. This degrades the performance in energy harvesting applications where multiple or broad-band absorption is necessary to enhance the conversion efficiency [13]. Therefore, efforts have gone into obtaining multiple- or broad-band absorbing structures [14–16]. These structures are designed by elaborately arranging the metallic resonant patterns or vertically stacking multiple metal-dielectric layers with different geometrical dimensions. However, multiple- or broad-band absorbing structures tuned by the dielectric spacing layer have not been reported as yet.

In this paper, we propose a dual-band mid-infrared metamaterial absorber tuned by the dielectric spacing layer in order to acquire more infrared radiation energy. Two pairs of circular-patterned metal-dielectric stacks are employed to excite the dual-band absorption peaks. The current distributions at the two resonances reveal that the enhanced electromagnetic field is established in the upper and lower resonant stack, respectively. The absorption peaks of the proposed structure remain quite high even at large incident angles, which could provide more efficient absorption for the oblique incident light.

2. Structure design

A schematic of the proposed dual-band MM absorber is shown in Fig. 1. It contains five functional layers: two pairs of circular-patterned metal-dielectric stacks and a metallic ground plane. The metallic layers are made of Al and separated by distinct dielectric spacing layers. The diameter of the circular pattern is denoted by d

*Corresponding author. Tel.: +86 28 83201574; fax: 86 28 83201575.
E-mail address: phzhou@uestc.edu.cn (P. Zhou).
Peer review under responsibility of Chinese Materials Research Society.

Production and hosting by Elsevier

http://dx.doi.org/10.1016/j.pnsc.2014.03.005
1002-0071/

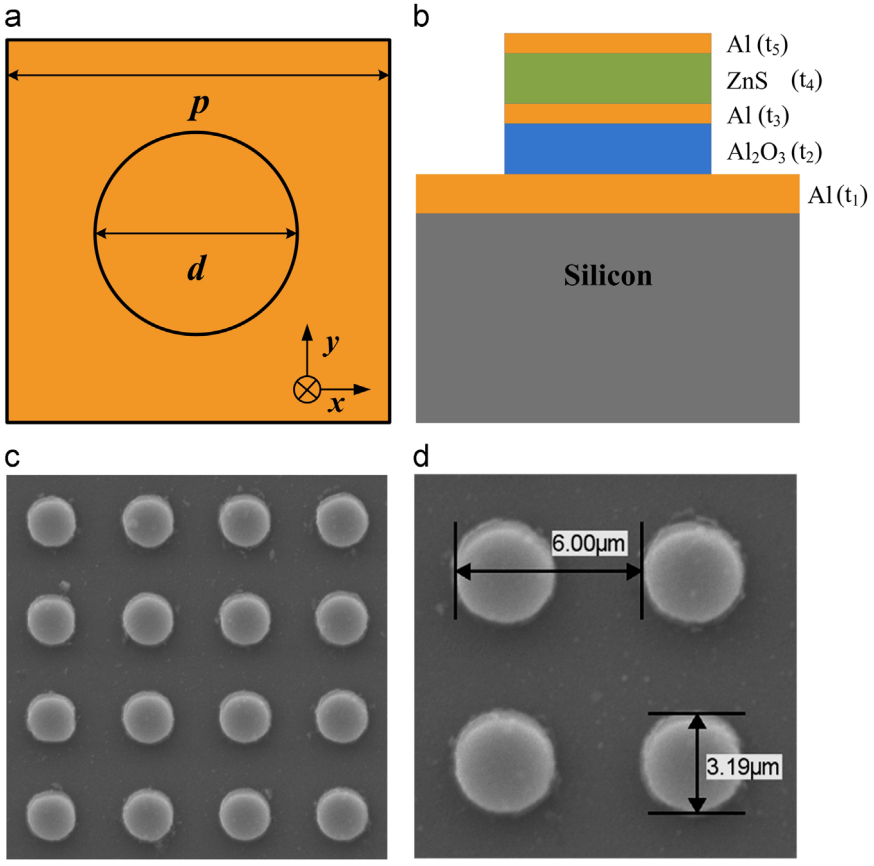

Fig. 1. Schematic of the dual-band MM absorber; (a) top view and (b) side view of the structure; (c) and (d) scanning electron microscopy (SEM) images of the dual-band MM absorber.

and the period of the unit cell by p. The thickness of the dielectric spacing layers is represented by t_2 and t_4, and the thickness of the metallic layers by t_1, t_3, and t_5. Since the electromagnetic response of the absorber is designed by the tuning of the dielectric spacing layer, we first perform numerical simulations [17] to investigate the relationship between the resonant absorption and the dielectric spacing layer.

3. Results and discussion

In the simulations, the complex permittivity of Al is described by the Drude model with a plasma frequency $\omega_p = 2 \times 3.57 \times 10^{15}$ rad/s and collision frequency $\omega_c = 2 \times 19.41 \times 10^{12}$ rad/s [18]. A normal incident TEM plane wave illuminates the structure with its polarization along the x-direction as shown in Fig. 1. The frequency-dependent absorption was obtained from the S-parameters by $A(\omega) = 1 - T(\omega) - R(\omega) = 1 - |S_{21}|^2 - |S_{11}|^2$, where $T(\omega)$ and $R(\omega)$ are the frequency-dependent transmission and the reflection, respectively. Fig. 2 presents the evolution of the maximum absorption and correspondingly the resonant absorption peak wavelength as a function of the dielectric constant ε' with structure parameters $p = 6$ μm, $d = 3.2$ μm, $t_1 = 200$ nm, $t_3 = t_5 = 100$ nm, $t_2 = 200$ nm, and $t_4 = 250$ nm. In Fig. 2(a) and (b), dielectric constant of the dielectric spacing layer in the lower resonant stack (ε_1') is set to 2, while dielectric constant of the dielectric spacing layer in the upper resonant stack (ε_2') varies from 3 to 9. For $\varepsilon_1' = 2$ and $\varepsilon_2' = 3$, there are two high absorption peaks located at 8.62 μm and 9.88 μm, respectively. As ε_2' increases from 3 to 9, the absorption peaks at longer wavelength (S_2) move from 9.88 μm to 16.63 μm, with the absorption magnitude initially increasing, reaching a maximum, and then decreases. Meanwhile, the absorption peaks at shorter wavelength (S_1) are almost unchanged except for a slight variation in the absorption magnitude. In Fig. 2(c) and (d), ε_1' varies from 2.5 to 5.5, and ε_2' is set to 9. For this case, the absorption peaks at longer wavelength (S_2) stay around 16.5 μm, while the absorption peaks at shorter wavelength (S_1) move from 9.38 μm to 13.13 μm, with the same variation tendency in the absorption magnitude as shown in Fig. 2(b). The simulation results reveal that the two absorption peaks in the dual-band absorber are contributed and tuned by the dielectric spacing layers in the upper and lower resonant stack, respectively. It appears that the resonance wavelength is quite sensitive to ε', and the dependency is nearly linear [19]. The variation in the absorption magnitude reflects the degree of impedance matching between the structure ($Z = \sqrt{\mu/\varepsilon}$) and free space ($Z_0$). By tuning the dielectric constant, impedance matching could be achieved and near perfect dual-band absorption obtained.

Another experimental parameter of the dielectric spacing layer that can be modulated is its thickness. Fig. 3 shows the evolution of the maximum absorption and correspondingly

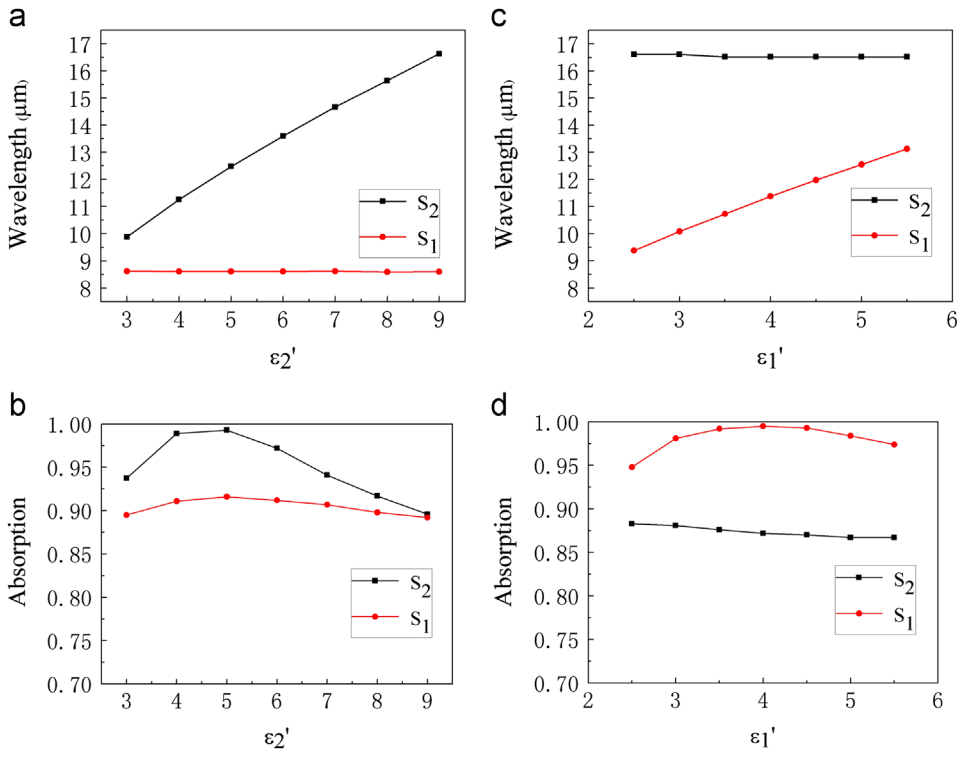

Fig. 2. The resonant absorption peak wavelength and correspondingly the maximum absorption as a function of the dielectric constant. (a) and (b) $\varepsilon_2^{'}$ varies from 3 to 9, and (c) and (d) $\varepsilon_1^{'}$ varies from 2.5 to 5.5, with structure parameters $p=6$ μm, $d=3.2$ μm, $t_1=200$ nm, $t_3=t_5=100$ nm, $t_2=200$ nm, and $t_4=250$ nm.

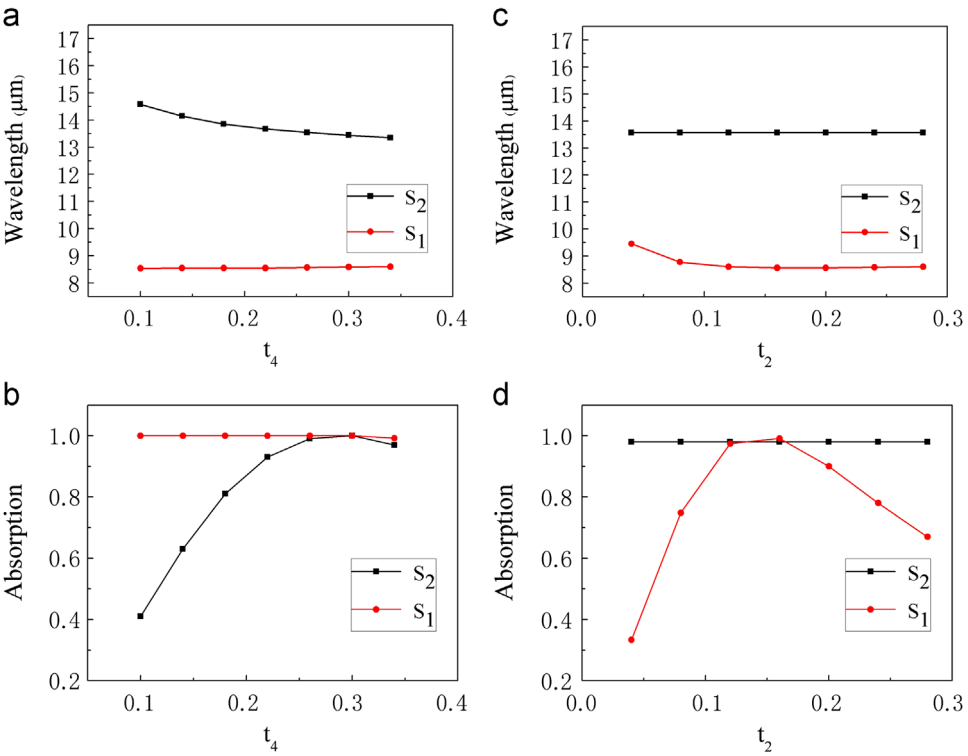

Fig. 3. The resonant absorption peak wavelength and correspondingly the maximum absorption as a function of the dielectric spacing layer. (a) and (b) t_4 varies from 100 nm to 340 nm with structure parameters $p=6$ μm, $d=3.2$ μm, $t_3=t_5=100$ nm, $t_2=250$ nm, and $t_1=200$ nm, and (c) and (d) t_2 varies from 40 nm to 280 nm with structure parameters $p=6$ μm, $d=3.2$ μm, $t_3=t_5=100$ nm, $t_4=250$ nm, and $t_1=200$ nm.

the resonant absorption peak wavelength as a function of the dielectric spacer thickness.

As shown in Fig. 3(a) and (b), both the resonant wavelength and the magnitude of absorption peaks at longer wavelength (S_2) vary with the thickness of t_4, with structure parameters $p=6$ μm, $d=3.2$ μm, $t_3=t_5=100$ nm, $t_2=250$, $t_1=200$ nm, and dielectric constant $\varepsilon_1^{'}=2$ and $\varepsilon_2^{'}=6$. Meanwhile, the absorption peaks at shorter wavelength (S_1) are almost unchanged. There exists an optimal thickness of the dielectric spacing layer that maximizes the absorption. For the present structural dimension, when $t_4=0.26$ μm, an absorption peak up to 99.9% at 13.54 μm could be achieved. The evolution of the resonant absorption presented in Fig. 3(a) reflects the variation of the near-field plasmon coupling in the resonant stack caused by the changing of the thickness of the dielectric spacing layer [20]. Similar trends are found in varying the thickness of t_2 as shown in Fig. 3(c) and (d).

As discussed above, we chose Al_2O_3 ($\varepsilon_1^{'}=2.28$) and ZnS ($\varepsilon_1^{'}=4.48$) as the dielectric spacing layers in the upper and lower resonant stacks, with structure parameters $p=6$ μm, $d=3.2$ μm, $t_1=200$ nm, $t_3=t_5=100$ nm, and $t_2=t_4=250$ nm. Fig. 4(a) presents the simulated absorption spectrum of the dual-band MM absorber (sample A) at normal incidence. As shown in Fig. 4(a), there are two distinct near-unity absorption peaks located at 9.03 and 11.83 μm. To explore the origin of the dual-band absorption, MM absorbers with a single Al_2O_3 (sample B) or ZnS (sample C) dielectric spacing layer were also studied. The thickness of the dielectric and metallic layers was the same in the three cases. As can be seen in Fig. 4(a), the absorption peaks of samples B and C are located at 8.83 and 12.11 μm, respectively. It is revealed that when the two single-dielectric-layer structures are stacked together, their resonant peaks both survive due to the hybridization of resonances within the two resonant stacks. There is a small redshift about 0.3 μm between the single- and dual-band absorption spectra. The distinction was caused by the loading effect between the upper and lower resonant stacks of the dual-band structure.

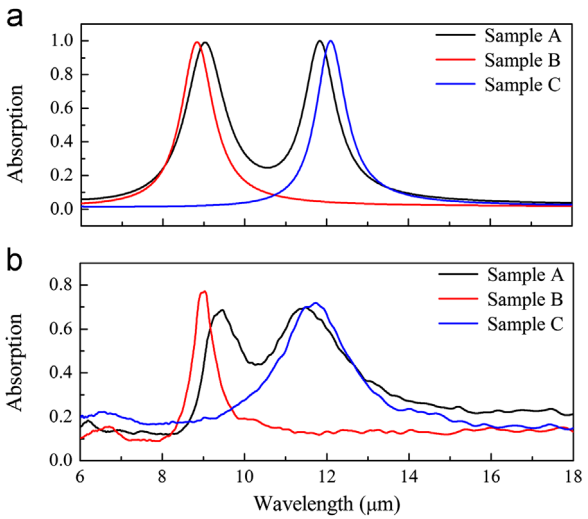

Fig. 4. (a) Simulated and (b) experimental absorption spectra of samples A–C.

The samples were prepared by standard *e*-beam deposition and UV lithography techniques. A 200 nm Al metallic ground plane was first evaporated onto a silicon substrate by *e*-beam deposition. This was followed by UV lithography to define the multiple patterned layers. The 250 nm dielectric (Al_2O_3/ZnS) films and 100 nm Al films were then deposited alternately. The pattern transfer was completed by a metal lift-off process. Scanning electron microscopy (SEM) images of sample A are shown in Fig. 1(c) and (d), illustrating the well-patterned products. A Bruker Tensor 27 Fourier transform IR spectrometer was used to measure the reflection spectra. The measured absorption spectrum of the dual-band MM absorber (sample A) is shown in Fig. 4(b). The dual-band absorption peaks are obtained at 9.43 and 11.42 μm with the absorption magnitudes of 69% and 70%, which are lower than the simulated values of 99% and 98%. The discrepancies stem from the fabrication tolerance, measurement limitation [21] and the inconformity of the dielectric constant of the dielectric spacing layer used in the simulation compared with the actual material parameters. The single-band absorbers (samples B and C) were prepared for comparison, and the measured absorption spectra were also plotted in Fig. 4(b). It is clear that the dual-band absorption originates from the stacking of two single-band absorption structures.

The total absorbed energy efficiency is the integration of absorption $A(\omega)$ over the total incident energy at the regarded energy band, that is, $\Delta=\int_{\omega_1}^{\omega_2}A(\omega)d\omega/(\omega_2-\omega_1)$, which present the overall capability of light conversion. In the energy band corresponding to the atmospheric window range from 8 to 14 μm, Δ is 45.2% for our dual-band absorption structure. This means that nearly half of the incident light within the considered range could be absorbed. Besides, Δ of the dual-band absorption structure is remarkably higher than the single-band absorption structure (sample A), and the value $\Delta=21.1\%$. Therefore, our dual-band absorption structure could acquire more of the incident energy compared with the single-band absorption structure, which will benefit the applications for thermal absorbing and light harvesting.

To gain a better understanding of the dual-band absorption mechanism, the current distributions at two resonance wavelengths were presented in Fig. 5. Simulation results reveal that the anti-parallel currents excited in the lower and upper resonant stacks correspond to the absorption peaks at 9.03 μm and 11.83 μm, respectively. The magnetic moment caused by the circulating current can strongly interact with the magnetic field of the incident light. As a result, the enhanced electromagnetic field is established in each resonant stack and most of the light could be dissipated [10]. Besides, at the resonance wavelength, the circulating current was only confined in one resonant stack, so the interaction between two resonant stacks could be neglected. This also explains why the absorption peak can be tuned independently by varying the dielectric spacing layer in the corresponding resonant stack.

The absorption performance at non-normal incidence is quite important in practical applications. In many cases, most of the possible incident light needs to be absorbed even at large incident angles. So we also carried out simulations to investigate the angle dependence of the dual-band absorber to evaluate its absorption performance at oblique incidence.

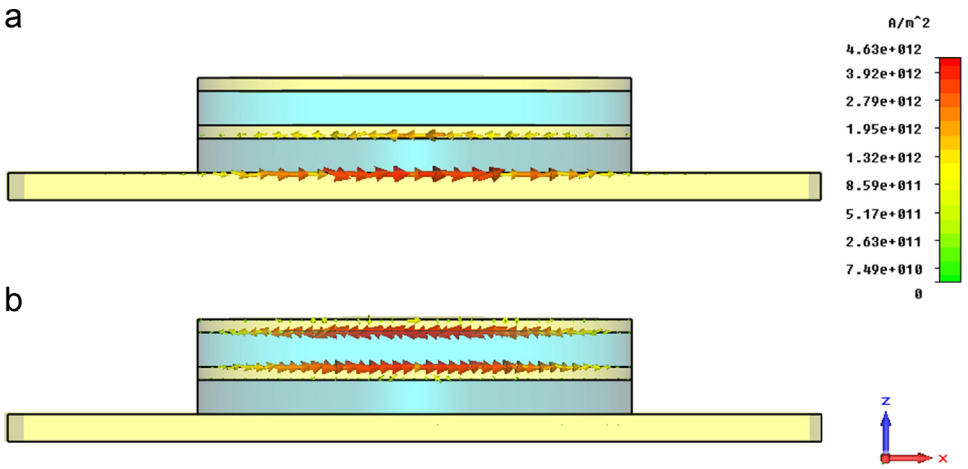

Fig. 5. Current distributions in sample A in the x–z plane at $y=0$ at two resonance wavelengths: (a) the absorption peak at 9.03 μm, and (b) the absorption peak at 11.83 μm.

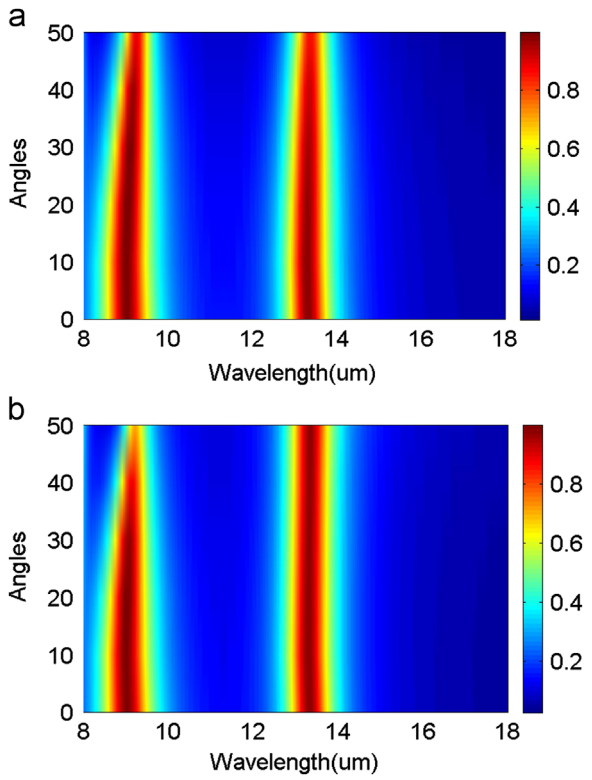

Fig. 6. Absorbance as a function of wavelength and the angle of incidence for (a) TE and (b) TM polarization incident light.

Fig. 6 shows the absorption spectra as a function of both wavelength and incident angles under TE ($E\perp x$–z plane) and TM ($E\perp y$–z plane) polarization. For both configurations, the dual-band absorption characteristics can be sustained by increasing the incident angle. More than 80% absorption is still obtained at center frequencies for both resonant peaks up to 40°. However, when the incident angle is beyond 40°, there is a decrease in the absorption magnitude and a shift in the peak position. Nevertheless, these simulations reveal that the proposed dual-band absorber operates quite well for both TE and TM configurations over a wide range of incident angles.

4. Summary

In summary, we have designed and fabricated a dual-band MM absorber in the mid-infrared regime by using a multilayer absorbing structure. The dual-band absorption is obtained from the stacking of two single-band absorption structures, and the absorption peak can be tuned by the dielectric spacing layer. The proposed structure could improve the energy absorption efficiency and operates quite well at large incident angles. Our study is expected to have multiple application advantages in thermal absorbing and light harvesting.

Acknowledgments

This work was supported by the National Natural Science Foundation of China (Grant nos. 61001026 and 51025208) and the Fundamental Research Funds for the Central Universities.

References

[1] M.C.K. Wiltshire, J.B. Pendry, I.R. Young, D.J. Larkman, D.J. Gilderdale, J.V. Hajnal, Science 291 (2001) 849–851.
[2] D.R. Smith, N. Kroll, Phys. Rev. Lett. 85 (2000) 2933.
[3] M. Gokkavas, K. Guven, I. Bulu, K. Aydin, R.S. Penciu, M. Kafesaki, C.M. Soukoulis, E. Ozbay, Phys. Rev. B 73 (2006) 193103.
[4] H. Tao, C.M. Bingham, A.C. Strikwerda, D. Pilon, D. Shrekenhamer, N.I. Landy, K. Fan, X. Zhang, W.J. Padilla, R.D. Averitt, Phys. Rev. B 78 (2008) 241103.
[5] S. Linden, C. Enkrich, M. Wegener, J.F. Zhou, T. Koschny, C.M. Soukoulis, Science 306 (2004) 1351–1353.
[6] S. Zhang, W.J. Fan, N.C. Panoiu, K.J. Malloy, R.M. Osgood, S.R.J. Brueck, Phys. Rev. Lett. 95 (2005) 137404.
[7] N. Liu, M. Mesch, T. Weiss, M. Hentschel, H. Giessen, Nano Lett. 10 (2010) 2342–2348.
[8] Y. Wang, T. Sun, T. Paudel, Y. Zhang, Z. Ren, K. Kempa, Nano Lett. 12 (2011) 440–445.
[9] J. Hao, L. Zhou, M. Qiu, Phys. Rev. B 83 (2011) 165107.
[10] X. Liu, T. Tyler, T. Starr, A.F. Starr, N.M. Jokerst, W.J. Padilla, Phys. Rev. Lett. 107 (2011) 045901.
[11] J.A. Mason, S. Smith, D. Wasserman, Appl. Phys. Lett. 98 (2011) 241105–241108.

[12] X. Liu, T. Starr, A.F. Starr, W.J. Padilla, Phys. Rev. Lett. 104 (2010) 207403.
[13] Y. Cui, K.H. Fung, J. Xu, H.M. Jin, S. He, N.X. Fang, Nano Lett. 12 (2012) 1443–1447.
[14] B. Zhang, Y. Zhao, Q. Hao, B. Kiraly, I. Khoo, S. Chen, T.J. Huang, Opt. Express 19 (2011) 15221–15228.
[15] S. Chen, H. Cheng, H. Yang, J. Li, X. Duan, C. Gu, J. Tian, Appl. Phys. Lett. 99 (2011) 253104–253107.
[16] Y.Q. Ye, Y. Jin, S. He, J. Opt. Soc. Am. B 27 (2010) 498.
[17] CST Microwave Studio, Computer Simulation Technology GmbH, Darmstadt, Germany, 2009.
[18] E.D. Palik, Handbook of Optical Constants of Solids, Academic Press, 1991, p. 370–406.
[19] G. Lévêque, O.J.F. Martin, Opt. Lett. 31 (2006) 2750–2752.
[20] J. Hao, J. Wang, X. Liu, W.J. Padilla, L. Zhou, M. Qiu, Appl. Phys. Lett. 96 (2010) 251104–251107.
[21] H. Tao, C.M. Bingham, D. Pilon, K. Fan, A.C. Strikwerda, D. Shrekenhamer, W.J. Padilla, X. Zhang, R.D. Averitt, J. Phys. D: Appl. Phys. 43 (2010) 225102.